

**RESEARCH ARTICLE**

# Causal Discovery to Understand Hot Corrosion

Akhil Varghese | Miguel Arana-Catania\* | Stefano Mori | Adriana Encinas-Oropesa | Joy Sumner

<sup>1</sup>Cranfield University, UK**Correspondence**\*Miguel Arana-Catania. Email:  
miguel.aranacatania@cranfield.ac.uk

Gas turbine superalloys experience hot corrosion, driven by factors including corrosive deposit flux, temperature, gas composition, and component material. The full mechanism still needs clarification and research often focuses on laboratory work. As such, there is interest in causal discovery to confirm the significance of factors and identify potential missing causal relationships or co-dependencies between these factors. The causal discovery algorithm Fast Causal Inference (FCI) has been trialled on a small set of laboratory data, with the outputs evaluated for their significance to corrosion propagation, and compared to existing mechanistic understanding. FCI identified the salt deposition flux as the most influential corrosion variable for this limited dataset. However, HCl was the second most influential for pitting regions, compared to temperature for more uniformly corroding regions. Thus FCI generated causal links aligned with literature from a randomised corrosion dataset, while also identifying the presence of two different degradation modes in operation.

**KEYWORDS:**

Gas Turbine superalloys, Hot Corrosion, Causal Inference, Causal Discovery Method, FCI Algorithm, Kernel-based Conditional Independence Test

## 1 | INTRODUCTION

Gas turbines are used to generate power and provide thrust<sup>[1]</sup>. In 2023 between 26% and 37% of UK electricity was generated from natural gas combustion, with gas turbines now shifting towards zero emission fuels such as H<sub>2</sub> or NH<sub>3</sub>, to meet UN goals. In order to increase the efficiency, gas turbines operate in a combined cycle with steam turbines, and are required to operate at higher temperatures and pressures, generating a more challenging environment for the materials used for their manufacture. Furthermore, contaminants such as sulphates, halides, and chlorides, contained in the fuel, together with salt impurities from the air, can create a highly corrosive environment<sup>[2]</sup>. Deposition of such contaminants on to the gas turbine's component blades and vanes gives rise to a corrosion mechanism called "hot corrosion", which adversely affects the service life of the gas turbines. Depending on the operating temperature conditions inside the gas turbine, Type-I or Type-II hot corrosion can occur<sup>[3]</sup>. Type-I and Type-II

hot corrosion are temperature-dependent and deposit-induced corrosion mechanisms that occur across the approximate temperature ranges of 850-950°C and 650-800°C, respectively<sup>[2]</sup>. Melting temperatures of the salt contaminants influence both these types of accelerated corrosion mechanisms but factors such as a high partial pressure of SO<sub>3</sub> are crucial for Type-II hot corrosion to occur<sup>[2]</sup>. While it is known that factors like operating temperatures, melting temperatures of salt contaminants, the deposition rate of the flux on gas turbine surface, partial pressures of gas contaminants, and material and gas compositions lead to hot corrosion in gas turbines, the exact variation of the underlying mechanism with changing parameters needs clarification.

Moreover, the degree of co-dependence and independence between these factors will help in understanding the influence that each factor has on hot corrosion. Hence, Causal Discovery<sup>[4,5]</sup> has been introduced to understand the causal relationships between the different corrosion factors from a statistical approach. These data-driven, causal relationships will help in understanding the underlying causal relationships of

each corrosion variable, and thus clarifying the physical corrosion mechanism. Such findings from this early-stage study can also help in designing future hot corrosion experiments, both in terms of the variables and their values, and can become the foundation upon which a predictive maintenance model can be developed.

## 1.1 | Hot Corrosion

Hot corrosion is a type of material degradation which is induced by the deposition of contaminants contained in the exhaust stream of a gas turbine<sup>[6]</sup>. These deposits are usually formed by alkali compounds that can increase the corrosion rates if in molten state<sup>[3]</sup>. Some of the contaminants come from the air intake (such as sodium, potassium, calcium), while others come from the fuel. The amount of deposition influences the corrosion rate of the materials in such environments<sup>[7]</sup>. Based on the operating temperatures and the type of contaminant attack, hot corrosion can be further divided into Type-I and Type-II hot corrosion:

### 1.1.1 | Type-I Hot Corrosion (High-temperature Hot Corrosion)

Type-I hot corrosion is also called high-temperature hot corrosion (HTHC) because it occurs within the temperature range of 850-950°C<sup>[2]</sup>. Various compounds can form, for example, Sodium from the ingested air and sulphur from the fuel could combine to form sodium sulphate ( $\text{Na}_2\text{SO}_4$ ), during the combustion cycle of the gas turbine<sup>[8][9]</sup>. The sodium sulphate could then condense onto the colder blading, and form a liquid (molten) salt, which initiates Type-I hot corrosion. In the presence of further impurities, such as NaCl from the industrial or marine atmosphere combines or K from sea droplets<sup>[9]</sup>, the formation of mixtures with lower melting points could occur which extend the temperature range of Type-I hot corrosion<sup>[10]</sup>.

Using a fluxing reaction, these eutectic mixtures dissolve the protective layer of the superalloy and attack the base material. These mixtures shorten the incubation period. Type-I hot corrosion is characterised by internal sulfidation, depletion of protective layers formed by chromium or aluminium, and leads to severe metal loss from the base material, impacting the gas turbine life. Sulfidation can be seen in Figure 1 (b) and (d).

### 1.1.2 | Type-II Hot Corrosion (Low-temperature Hot Corrosion)

Type-II hot corrosion, also called low-temperature hot corrosion (LTHC), occurs at temperatures between 650-800°C<sup>[3]</sup>. As in the case of Type-I hot corrosion, the formation of a

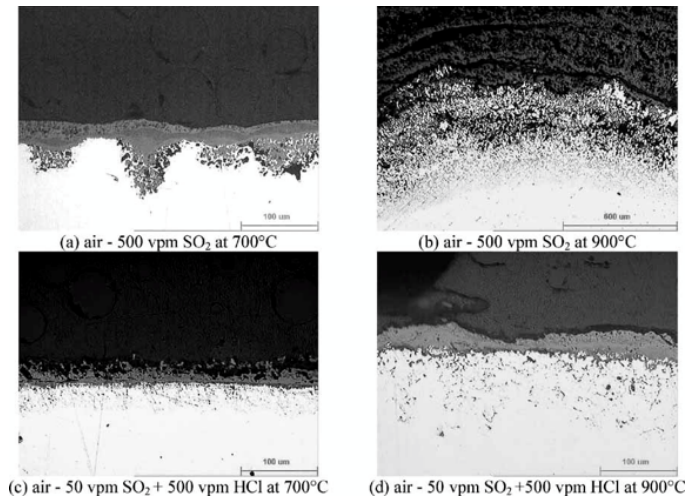


**FIGURE 1** Optical micrographs of SC<sup>2</sup>-B exposed for 500h with a flux of 5  $\mu\text{g}/\text{cm}^2/\text{h}$ . The picture shows pitting attack and scale formation at 700 and 900 °C<sup>[11]</sup>.

molten deposit is also involved in the mechanism controlling the corrosion behaviour. However, the mechanism occurs at temperatures below the melting temperature of many pure salts. In Type-II hot corrosion the  $\text{Na}_2\text{SO}_4$  forms mixtures with metallic inorganic compounds<sup>[2]</sup>, which lowers the combined melting temperature and initiates the corrosion process. These inorganic metal compounds are formed by  $\text{SO}_3$  present in the combustion gas and the metal<sup>[10]</sup>, making Type-II hot corrosion not only a function of the temperature, but also a function of the partial pressure of the  $\text{SO}_3$  gas<sup>[3]</sup>. Type-II hot corrosion is characterised by pitting with localized failure as seen in Figure 1 (a)<sup>[2]</sup>. The cause of pitting initiation is currently under consideration and has been linked to a wide range of factors including grain boundaries, precipitates, gas environment and the salt deposit.

## 1.2 | Gas Turbine Materials

To increase efficiency, higher turbine operating temperatures and pressures are required. This has driven the formulation and selection of materials to be used, which need to have<sup>[10]</sup>:

- high mechanical strength at temperatures close to the melting point
- high creep resistance
- high corrosion resistance

For these reasons “superalloys” with better mechanical properties than conventional alloys have been developed. These alloys are nickel-, iron-nickel and cobalt-based<sup>[12]</sup>, with other elements in solution, such as chromium and aluminium,

which preferentially oxidise to form a thin protective oxide layer to provide resistance to corrosion and oxidation<sup>[12]</sup>.

To ensure resistance to hot corrosion, a minimum amount of chromium is needed, for instance, 22% chromium is present in Co-base Haynes 188 superalloy, which provides high fatigue strength and strong resistance to hot corrosion<sup>[13]</sup>. In comparison, even though nickel-base Haynes 214 contains 16% chromium, it provides high oxidation resistance to temperatures above 900°C due to the presence of 4.5% aluminium<sup>[12]</sup>.

Microstructure can also be controlled with commercially used single crystal superalloys like CMSX-11C and SC-16 providing increased resistance to hot corrosion due to the presence of more than 12% chromium<sup>[6]</sup>.

### 1.2.1 | Protective Coatings

Despite the more recent advancements, most of the superalloys are not able to provide the desired lifetime in all conditions within gas turbines. Thus, for specific areas of the turbines, coatings are required<sup>[6,12]</sup>. Aluminide diffusion coatings, overlay coatings and thermal barrier coatings are the most used types of coatings for gas turbine applications<sup>[14]</sup>. Platinum-modified aluminide (Pt-Al) coatings like RT-22 and CN-91 are widely used<sup>[15]</sup> due to their great resistance to Type-I and Type-II hot corrosion<sup>[16]</sup>. On the other hand, overlay coatings provide excellent oxidation and hot corrosion resistance due to their ability to form alumina and chromia scales<sup>[17]</sup>. Figure 2 shows the degradation resistance of a platinum-aluminide diffusion coating versus three overlay coatings<sup>[8]</sup>.

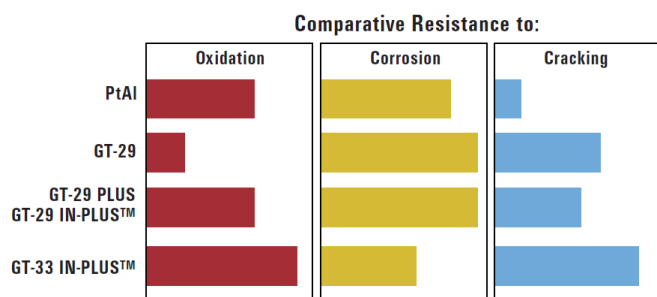


**FIGURE 2** Comparison of resistance performance between platinum-aluminide, and overlay coatings<sup>[8]</sup>

### 1.2.2 | Hot Corrosion summary

Hot corrosion is dependent on different factors including the chemistry of the corroding material, temperature, partial pressure of contaminants and chemistry of the contaminants. For

this reason, it is not straightforward to understand the connection between the different parameters and the rates of corrosion. Understanding the cause-effect relationship between the corrosion factors discussed can help in analysing materials' degradation in gas turbines. The discovery of cause-effect relationships can be done through the use of causal discovery techniques, which can investigate the links between these corrosion factors.

## 1.3 | Causal Discovery

Causal analysis techniques have been prominently used in the fields of engineering, medicine, and economics<sup>[4]</sup>. Manufacturing, however, has yet to fully embrace causal discovery methods when compared to the previous fields, and thus there is limited work on hot corrosion using these techniques<sup>[18]</sup>.

One example of the use of causal discovery methods was applied to detect strong relationships in degradation data<sup>[19]</sup>. A neural network was used to assess the degradation state of some equipment. The causal discovery method FCI was used to create a model of the relationship between the variables. The variables responsible for the degradation state found using FCI, were then fed into Long Short Term Memory (LSTM) neural networks for the subsequent assessment. In this manner, the data-driven model was trained, and its interpretability was improved.

In a second example<sup>[20]</sup>, the method was applied to the design process of energy-efficient buildings. The authors applied the causal discovery algorithm Greedy Equivalence Search (GES) to the variables that potentially affect building design. Creating such a causal framework is expected to allow designers, developers, and construction workers to inspect and continuously improve their own designs and construction methodology.

In the final example reported here, causal discovery algorithms were used on an Alzheimer's disease dataset<sup>[21]</sup>. The study compared between two causal discovery algorithms and an existing standard graph on Alzheimer's Disease, which was formed using literature and prior experience. FCI and Fast Greedy Equivalence Search were the methods used to form causal graphs, with initial causal graphs formed purely based on observational datasets i.e., without prior subject knowledge. Subsequently, 'background knowledge' was added to the algorithms and the changes in average accuracy, recall and precision were compared with the former results. These causal graphs were later validated based on the existing standard graph and the discovered graphs were found to be very close.

This research aims to understand the degree of influence, independence and co-dependence of several hot corrosion variables causing material degradation in a gas turbine setting using causal discovery techniques.

## 2 | METHODS

Section 2.1 explains the corrosion dataset along with its seven variables. Section 2.1.1 illustrates the arrangements and the necessary fine-tuning made to the dataset to use as input to the causal discovery algorithms. Section 2.2 explains the significance levels and the assumptions made for analysing the causal graphs during the discussion. Sections 2.2 to 2.5 explain the causal discovery algorithm and everything required for its implementation.

### 2.1 | Corrosion Data

The corrosion dataset used in this work was formed by Dr Adriana Encinas-Oropesa in 2005, during her Ph.D. thesis in collaboration with the Advanced Long Life Turbine Coating Systems project (ALLBATROS)<sup>[11]</sup>. To produce the corrosion dataset, experiments were conducted on a single crystal CMSX-4. Three different metallic protective coatings, RT22, CN91 and LCO22 were applied to the CMSX-4 base alloy. The uncoated CMSX-4 material and the three coated versions of the CMSX-4 alloy were treated as four different materials during the application of the causal discovery algorithm. The dataset consists of two different operating temperatures, 700 and 900°C, with varying levels of gas compositions and deposit chemistries and fluxes.

After an exposure time of 1000 hours, the material loss data were collected. This data corresponded to three different flux deposition rates of 0.5, 1.5 and 5  $\mu\text{g}/\text{cm}^2/\text{h}$ . The gas composition consisted of a constant 300vppm (volumetric parts per million) of  $\text{SO}_2$  along with varying amounts of HCl (0 or 100vppm). Material loss values (due to hot corrosion) corresponding to each deposition rate, temperature, material, and amount of gas composition were tabulated.

#### 2.1.1 | Data Pre-Processing

To assess the extent of hot corrosion, pre- and post-exposure sample dimensions were compared resulting in 30 values. The dataset formed gives material loss as a function of the cumulative probability of each amount of metal loss. The probability indicates the likelihood of having a certain amount of metal loss or more. Thus, the most extensive damage occurs with low probability. For simplicity, the cumulatively distributed dataset was truncated to three values: highest, median, and lowest material loss. The highest and the lowest material loss (HML and LML) are used to understand the factors that are dominantly influencing the hot corrosion at the opposite ends of the material loss spectrum, while the median material loss (MML) helps in identifying the typical corrosion factors leading to hot corrosion from an overall perspective.

‘Amount of salt’, ‘Temperature’, ‘ $\text{SO}_2$ ’, ‘HCl’, ‘Time of exposure’, ‘Material’, and ‘Material Loss’ were the seven variables tabulated. Although the variables could take continuous values, in the experiments they were fixed to specific values. Thus all are considered categorical variables for the causal discovery algorithm, except for the case of the Material Loss which took different, continuous values.

### 2.2 | Statistical Independence Tests

The cause-effect relationship between the corrosion variables present in the dataset are analysed from a statistical point of view. The null hypothesis considered is a lack of any causal relationship. As such, results are presented with their significance level  $\alpha$ , which represents the probability of incorrectly rejecting the null hypothesis when it is true. The confidence level (CL) follows the relation  $\text{CL} = 1 - \alpha$ <sup>[22,23]</sup>.

Causal discovery methods use conditional independence tests (CIT) to identify causal links between the variables of the dataset and attempt to eliminate the spurious correlations within those variables<sup>[24]</sup>. The independence between the set of nodes  $X$  and  $Y$ , conditional to a set of nodes  $Z$ , is written as  $X \perp Y \mid Z$ <sup>[4]</sup>. The independence between variables can be inferred locally from the CIT, but also globally from the causal structures present in the graph and how they are connected. Analysing all the causal paths connecting any variables it can be inferred what is their causal relationship. A criterion commonly used in this regard is the d-separation of variables<sup>[4]</sup>.

Causal discovery algorithms use various statistical tests to assess the independence between variables, such as the Chi-squared  $\chi^2$  test (non-parametric test measuring the goodness-of-fit between expected and observed frequencies which works well with large discrete categorical samples)<sup>[25,26]</sup>, Fisher-Z test (used for partial and zero correlation, this parametric test assumes that the variables are normally distributed and works mainly on large sample sizes of continuous variables)<sup>[26,27]</sup>, G-squared test (non-parametric test that highlights relationships between categorical variables with more than two levels)<sup>[25]</sup>, or the Kernel-based conditional independence test (KCI). In this work, it was used the latter.

The KCI test is a non-parametric test that can be derived from the kernel matrices of the variables under consideration, which characterize the similarity of the samples of those variables<sup>[28,29]</sup>. These kernel functions recognise non-linear relationships between data points. This test can be applied to discrete or continuous variables. Figure 3 shows the evolution of the accuracy of the test as a function of the number of samples for the dataset analysed in the original publication of the method.

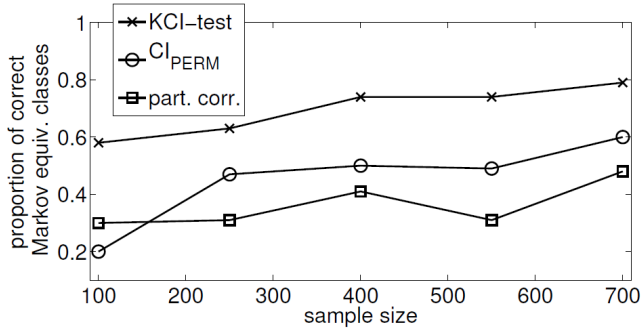


**FIGURE 3** Accuracy of different CITs to infer the correct Markov Equivalence Class as a function of the sample size<sup>[28]</sup>.

### 2.3 | Causal Links, Structures and Graphs

The different causal nature of the relationships between the variables can be represented with different types of causal links<sup>[30]</sup>, as illustrated in Table 1. The relationship depends on the variables measured and on possible confounding variables (those unmeasured variables which influence the underlying causal mechanism)<sup>[31]</sup>.

After applying the CIT to the variables from the dataset, the result of the causal discovery algorithm is a graphical representation of the causal links between the variables called a causal graph<sup>[30]</sup>. Chains, forks, and colliders (also called v-structures) are the three building blocks used in these causal graphical models to illustrate the cause-effect relationship between the variables.

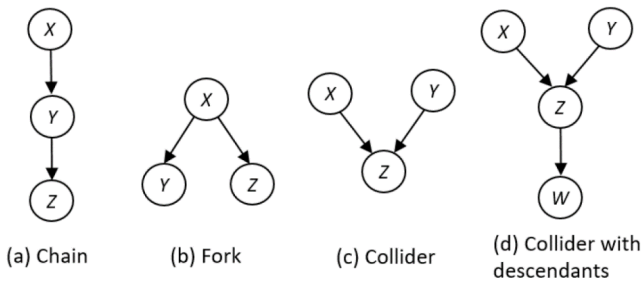


**FIGURE 4** Building blocks of a Causal Graph<sup>[30]</sup>

Figure 4 (a) shows the chain structure wherein  $X \rightarrow Y \rightarrow Z$  forms a chain where  $X$  causes  $Y$  and  $Y$  causes  $Z$ , therefore the conditional independence can be written as  $X \perp Z | Y$ <sup>[34]</sup>. Figure 4 (b) shows the fork structure  $Y \leftarrow X \rightarrow Z$  wherein the node  $X$  forms a directed edge towards  $Y$  and  $Z$  making it the common ancestor for  $Y$  and  $Z$ <sup>[34]</sup>. Since there is only one path between  $Y$  and  $Z$  through  $X$  based on the d-separation criterion, conditional independence can be written as  $Y \perp Z | X$ .

Figure 4 (c) shows a collider  $X \rightarrow Z \leftarrow Y$ , wherein the descendant  $Z$  has two common ancestors  $X$  and  $Y$ . Even though there is one path between  $X$  and  $Y$ , the presence of a collision node  $Z$  makes  $X$  and  $Y$  conditionally dependent given the collision node  $Z$ , i.e.  $X \not\perp Y | Z$ . Figure 4 (d) shows a collider structure with extra descendant  $W$  where  $X \not\perp Y | Z$  and  $X \perp Y | W$ .

A causal directed acyclic graph (DAG) consists of a set of random variables with edges between them which never form a directed cycle within the graph<sup>[4]</sup>. Generally, causal discovery algorithms do not allow identifying the causal graph, but the Markov Equivalence Class (MEC) of the graph. If two DAGs are Markov equivalent, they have the same skeleton and set of colliders as well as the same (conditional) independencies<sup>[24]</sup>, which is what the algorithms can usually identify. Once the class is identified, using interventions in the variables it is then possible to identify the actual causal DAG<sup>[35]</sup>.

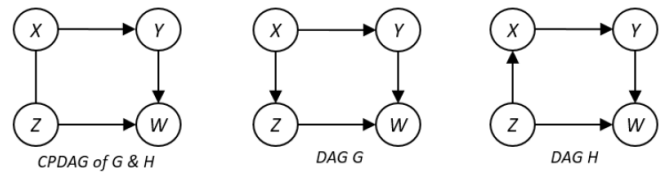


**FIGURE 5** Example of Markov Equivalence Class<sup>[30]</sup>

The example taken from<sup>[30]</sup> in Figure 5 shows a Completed Partially DAG (CPDAG) of  $G$  and  $H$  which represents the union of the Markov equivalent DAGs  $G$  and  $H$ . The undirected edge between  $X$  and  $Z$  in the CPDAG suggests that it might contain  $X \rightarrow Z$  (shown in the DAG  $G$ ) or  $Z \rightarrow X$  (shown in the DAG  $H$ ).

Table 2, shows the different edges that can be observed in each type of causal graph. Each causal discovery algorithm produces as an output a different type of causal graph.

### 2.4 | Causal Discovery Algorithms

The two main categories of causal discovery algorithms are constraint-based and score-based methods. The first checks the graph structure against the independence constraints imposed by the data. In the second method, possible graphs are scored for their ability to fit the data. In the latter, the space of DAGs is searched to find the graph that maximises the score. This last method is especially useful when dealing with a large number of variables since the combinatorial space of possible graphs grows exponentially. In this work, since a small number of variables are studied it is used a constraint-based method.

The constraint-based algorithms use CITs to investigate the type of edges between the variables or their absence<sup>[5]</sup>. One of the earliest and most common of these algorithms is the



**TABLE 1** Different types of causal links and their respective denotations ignoring any selection bias<sup>[31–33]</sup>

Causal Link		Description
$A \rightarrow B$ (directed)		A is the cause of B
$A - B$ (undirected)		Undetermined. A can cause B and B can cause A
$A \leftrightarrow B$ (bidirected)		A and B do not cause each other but have a latent common cause.
$A \circ \rightarrow B$ (partially directed)		Confounding variables between A and B A causes B (“o” turns into tail end)
$A \circ - \circ B$ (undirected with “o” ends)	$A \rightarrow B$	There exists a confounder between A and B (“o” turns into arrow end)
	$A \leftarrow B$	
	$A \rightarrow B$	A causes B
	$A \leftarrow B$	B causes A
$A \leftrightarrow B$		A and B do not cause each other. Confounder between A and B This last option can be also combined with the previous two

**TABLE 2** Causal Graphs and their types of edges<sup>[30,36–39]</sup>

	Directed ( $\rightarrow$ )	Undirected ( $-$ )	Bi-directed ( $\leftrightarrow$ )	Partially Directed ( $\circ \rightarrow$ )
DAG	X			
Partially DAG (PDAG)	X	X		
Completed PDAG (CPDAG)	X	X		
Maximal Ancestral Graph (MAG)	X	X	X	
Partial Ancestral Graph (PAG)	X	X	X	X

PC (Peter & Clark) Algorithm<sup>[40]</sup>. It uses CITs to understand the underlying causal mechanism of the causal structures. It assumes independent and identically distributed (i.i.d) samples and absence of confounding variables.

Here it is used the Fast Causal Inference (FCI) algorithm<sup>[40]</sup>. It is a variant of the PC algorithm that provides asymptotically correct results while considering the presence of confounding variables in a dataset with i.i.d samples<sup>[5]</sup>. The output causal graph of the FCI algorithm is a Partial Ancestral Graph (PAG), including the presence of directed, undirected, partially directed and bi-directed edges<sup>[30]</sup>.

## 2.5 | FCI Algorithm Implementation

The causal-learn<sup>1</sup> package<sup>[41]</sup> was used for implementing the FCI algorithm. The dataset used as the input of the FCI algorithm included the variables shown in Table 3 .

From the initial seven variables available, mentioned in section 2.1.1, SO<sub>2</sub> and Time of Exposure were removed from the dataset because of their constant values. The rest of the variables were used as input to the algorithm. The four materials used in the experiments were assigned numbers from 1 to 4, respectively. The algorithm was applied with the default parameter settings, CIT = KCI and no background knowledge.

Since the dataset consisted of only five variables, no background knowledge was introduced into the causal algorithm to avoid selection- or expert-bias. Therefore, the causal graphs formed were purely based on the observational data. A range of 1% to 99% significance level, with a 1% step increment, was implemented to observe how the causal links would form with high and low confidence levels.

## 3 | RESULTS

This section presents the causal graphs obtained by implementing the FCI algorithm on the material loss datasets. The descriptions of the algorithms, graphs and types of links can be found in Sections 2.3 and 2.4.

Based on the degree of material loss, the dataset was divided into three parts: Highest Material Loss (HML), Median Material Loss (MML) and Lowest Material Loss (LML) (see Table 3 ). Varying significance levels from 1% to 99% were considered in the FCI algorithm. The results are differentiated according to HML, MML and MML and the significance level of each graph.

Table 4 shows the causal graphs obtained by applying KCI in the FCI algorithm on the HML dataset. The “o” termination in the causal link formed between Amount of Salt and Material Loss at  $\alpha = 1\%$ , illustrates that it can be either an arrowhead ( $\rightarrow$ ) or a tail end of a directed edge (see Table 1 ). Hence, the

<sup>1</sup> <https://github.com/py-why/causal-learn>

**TABLE 3** Categories of variables present in the datasets for highest (HML), median (MML) and lowest (LML) material loss

Mat. Loss / Dataset	Materials				Temperature (°C)	Amount of Salt (µg/cm <sup>2</sup> /h)			HCl (ppm)		
HML	1	2	3	4	700	900	0.5	1.5	5.0	0	100
MML	1	2	3	4	700	900	0.5	1.5	5.0	0	100
LML	1	2	3	4	700	900	0.5	1.5	5.0	0	100

direction of the causal relationship is not clearly depicted at  $\alpha = 1\%$  between the two variables.

At  $\alpha = 7\%$ , partially directed edges “o→” from Amount of Salt and HCl to Material Loss were formed. This means that if “o” becomes an arrowhead, it forms a bidirected edge. Table 1 shows that the bidirected edge indicates that there is an unmeasured confounder present between the two variables. On the other hand, if “o” becomes a tail end, it confirms that Amount of Salt and HCl causes Material Loss. Similarly, Temperature and Material formed partially directed edges with Material Loss at  $\alpha = 8\%$  and  $\alpha = 60\%$  for HML conditions, respectively.

Table 5 shows the results for the MML dataset. The undirected edges with “o” ends which formed between Amount of Salt and Material Loss at  $\alpha = 1\%$ , get converted to a partially directed edge from Amount of Salt to Material Loss, along with a partially directed edge from Temperature to Material Loss at  $\alpha = 9\%$ . Gradually, partially directed edges were formed from HCl and Material to Material Loss at  $\alpha = 20\%$  and  $\alpha = 60\%$ , respectively.

The causal graphs for the LML dataset are presented in Table 6. At  $\alpha = 1\%$  for the LML dataset, an undirected edge with “o” ends was formed between Amount of Salt and Material Loss. With the increase in  $\alpha$  to 20%, 50% and 70%, partially directed edges were formed from Amount of Salt and Temperature, HCl and Material to Material Loss, respectively.

## 4 | DISCUSSION

In this section it is discussed the nature of the current corrosion dataset and its drawbacks, as well as the causal graphs formed by the FCI algorithm and their key findings.

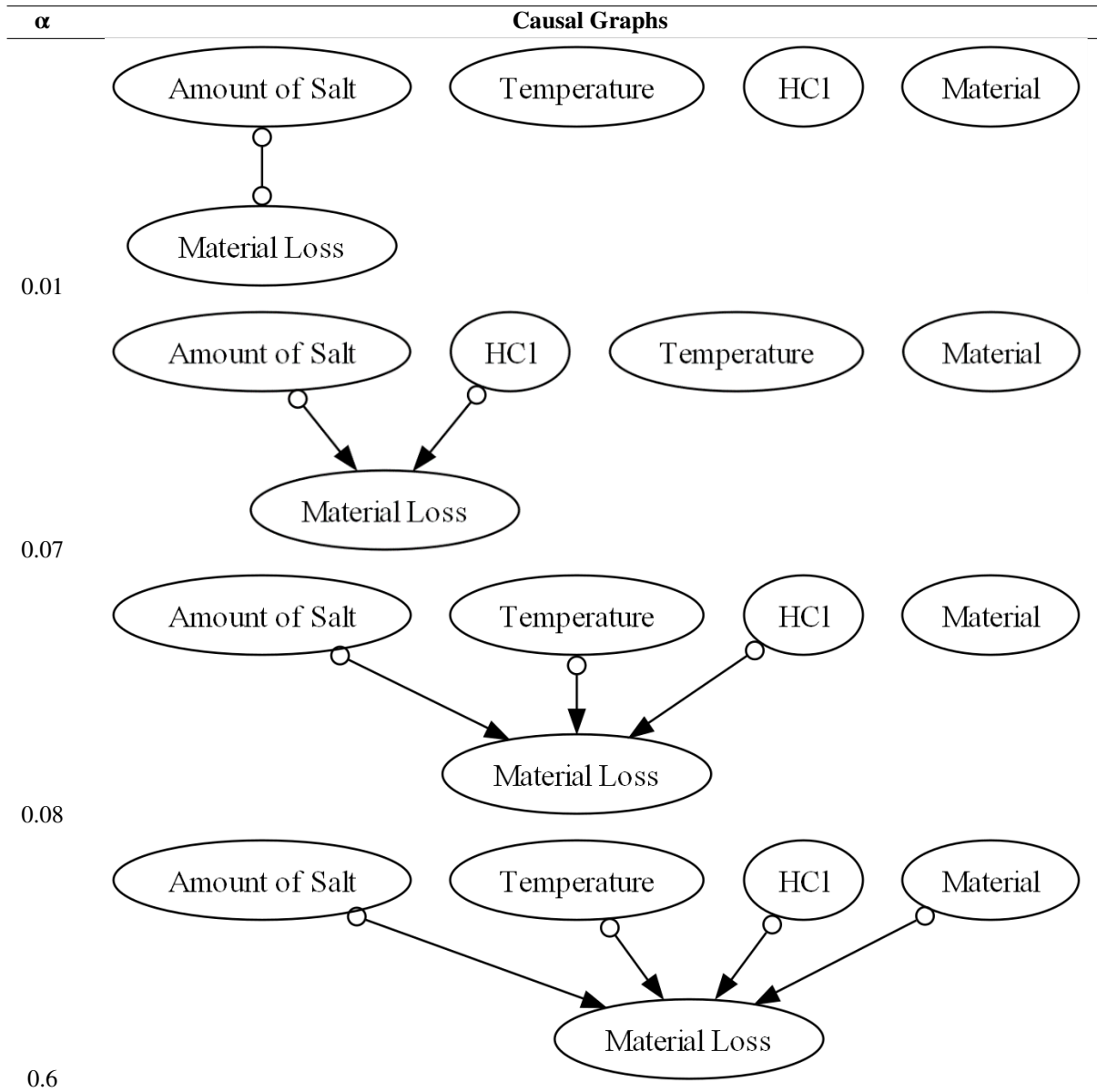
The type of dataset that is used as an input to the algorithm is one of the major factors determining the result. The current corrosion dataset was designed to maintain control over the corrosion variables to understand the effects on the material loss. The causal graphs in Tables 4 to 6, show that all the corrosion variables are directed towards Material Loss with increasing significance values. This means that the variables were controlled to observe the amount of material loss in the base material. However, for a pure causal inference study, randomisation in the variables would have offered a greater benefit<sup>[40]</sup>. For instance, if all the variables were uncontrolled

and randomised, observing causal links within the variables could have been a possibility. This would have helped in understanding the cause-effect relationship between the variables and not just through the Material Loss. The degree of influence that each variable has on Material Loss with varying significance levels can be observed in Tables 4 to 6. However, no claims can be made about the presence of causal relationships between ‘Amount of Salt’, ‘Temperature’, ‘HCl’, and ‘Material’ using the current dataset.

As discussed in sections 1.1.1 and 1.1.2, the salt deposition on the material surface is a significant factor in causing hot corrosion and, indeed, hot corrosion is also defined as a deposit-induced accelerated form of corrosion<sup>[3]</sup>. The salt deposits initiate the breakdown of the protective oxide layer of the substrate which is the starting point of hot corrosion<sup>[2]</sup>. Therefore, even at smaller significance values, Amount of Salt makes a directed or an undirected causal link with Material Loss for all the material loss levels (HML, MML, and LML).

Operating temperature facilitates the corrosive environment that enables hot corrosion<sup>[3]</sup>. Moreover, the lower melting point of the eutectic mixtures formed by different salts accelerates the corrosion process<sup>[2]</sup>, hence proving that temperature is another factor that has a significant influence on hot corrosion. Indeed, for MML and LML temperature becomes the second significant variable that influences hot corrosion in the given dataset, at smaller significance values. For MML and LML HCl in the gas only appears to form a causal link with Material Loss at higher significance levels. Chloride-contaminated oxide layers are known to accelerate the corrosion rate<sup>[42]</sup>. HCl is a crucial factor that participates in increasing hot corrosion rates. More experimental research is required to clarify the influence of HCl. However, this analysis shows its significance for driving extreme metal loss such as pitting.

Table 4, formed using the HML dataset, shows that at 1% significance level, the outcome from FCI shows an undirected causal link between Amount of Salt and Material Loss with “o” at either end. This means that at such a conservative significance value, FCI is only able to infer the existence of a link between the two variables without pointing out the cause-effect relationship. The undirected causal link can also point towards the probability of incorrectly accepting the null hypothesis i.e., Type-II error. The “o” ends can be perceived as an arrowhead or a tail end of a directed edge because the algorithm is too conservative in assigning them to form a meaningful causal link.

**TABLE 4** Causal graphs using KCI in FCI algorithm with increasing significance levels for HML dataset

In case both “o” ends become arrowheads, then it means that there is a confounding variable that has not been considered in the dataset.

In Table 4, with a significance value of 7%, the three partially directed ( $o \rightarrow$ ) causal links confirm that there is a possibility of Amount of Salt, HCl, and Temperature being factors causing Material Loss, or there exist unmeasured confounders between them that are influencing the behaviour of those variables. The FCI algorithm is not able to clarify the causal relationship between these variables and shows the possibility that confounder variables are present. HCl forms the same partially directed edge with Material Loss and a similar argument can be made for this causal link as well. Under

the specific conditions of the test, it seems that HCl is linked to HML, so it seems as HCl is one of the driving forces involved in the formation of pitting. This provides a very useful insight into the mechanism of hot corrosion, as the cause of pit initiation is still under debate. From  $\alpha = 7\%$ , Temperature also forms a partially directed causal link with Material Loss. This suggests that for the HML dataset, HCl and Temperature are the most influential factors advancing material loss, after Amount of Salt. There is also a possibility that unmeasured confounders exist which influence all the said variables. Therefore, datasets with a larger sample size and greater number of variables can further help in understanding the presence of these confounders.



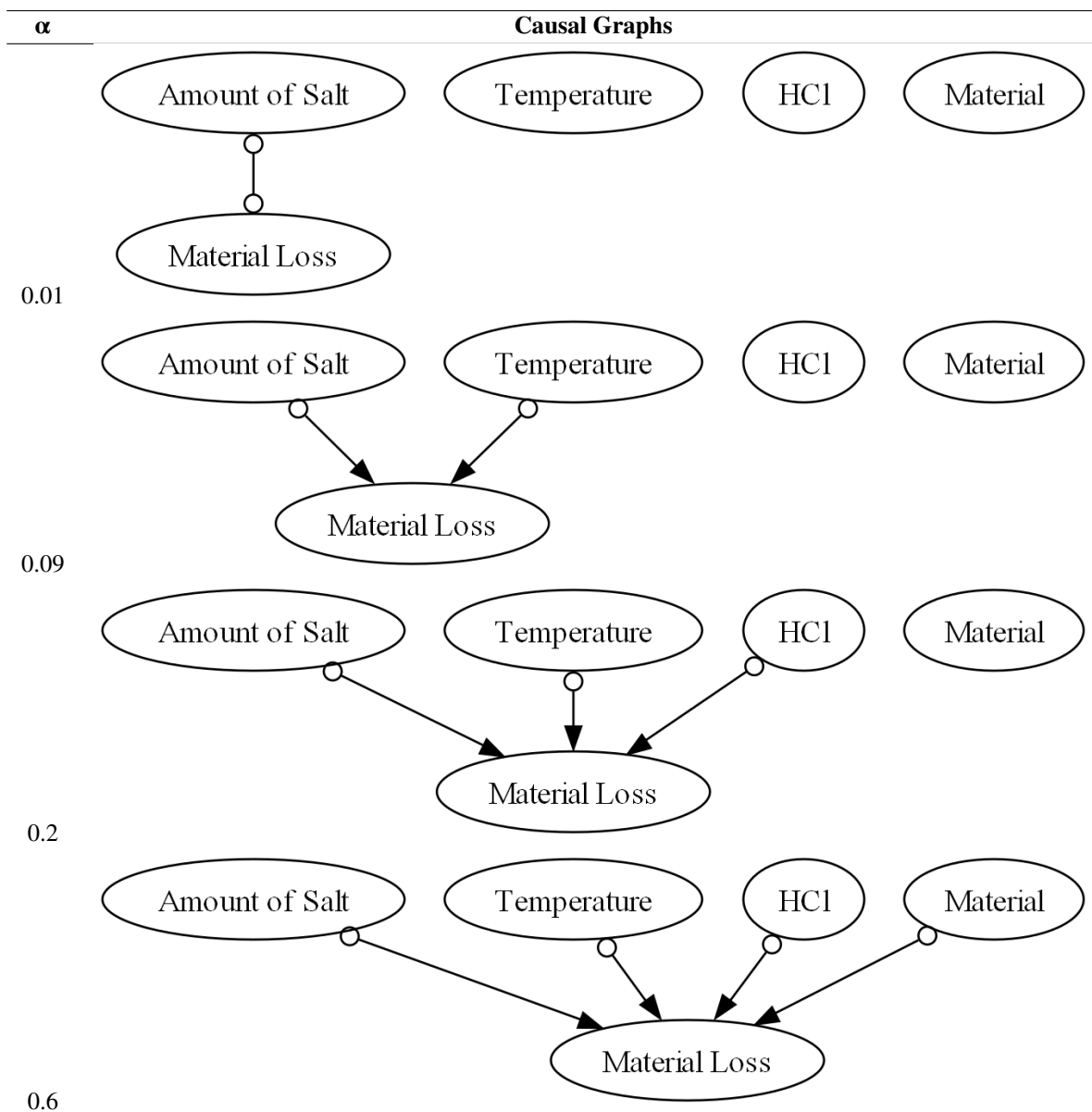
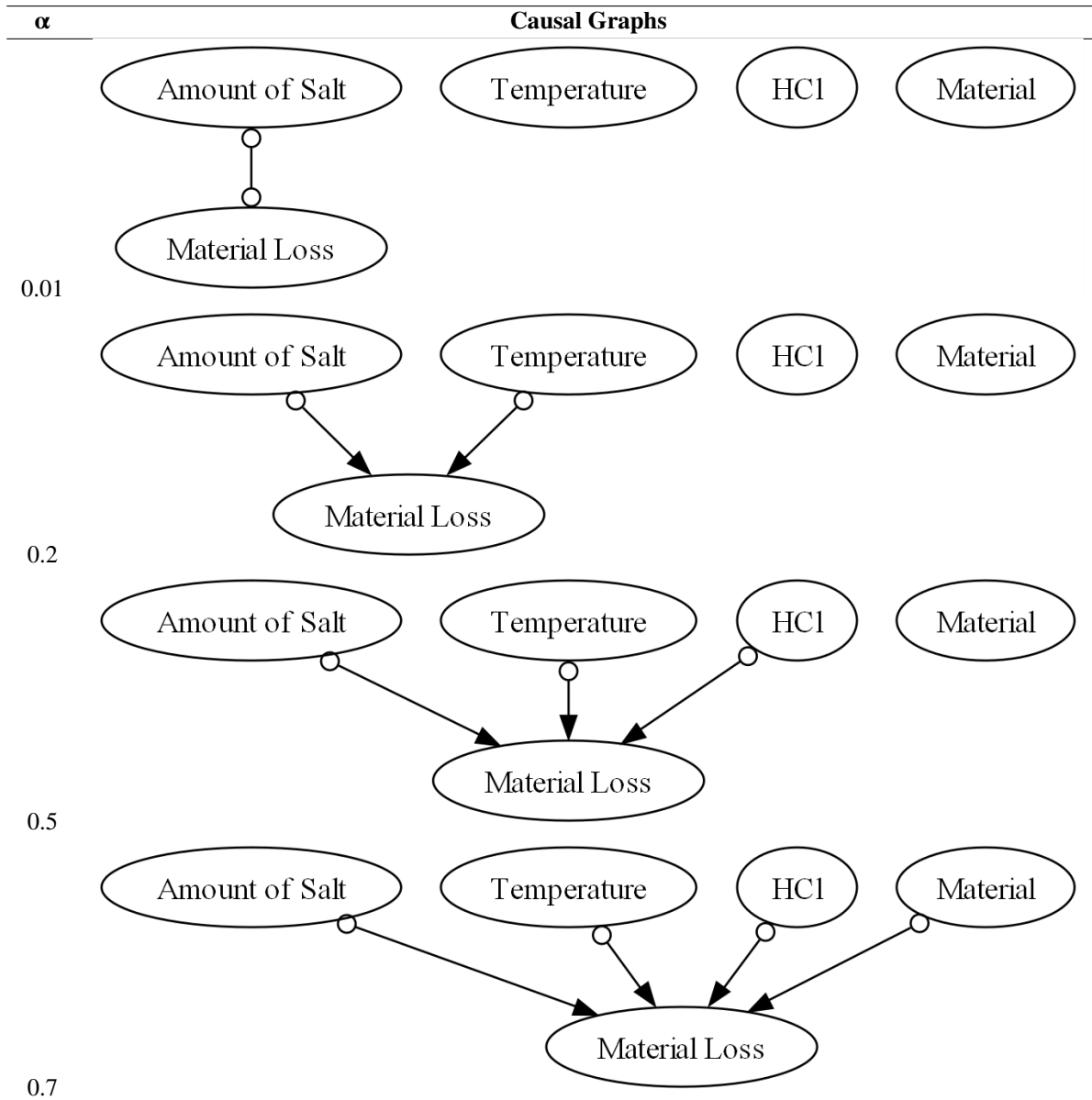
**TABLE 5** Causal graphs using KCI in FCI algorithm with increasing significance levels for MML dataset

Table 5 shows that the FCI algorithm is not confident enough in forming causal links between the variables up to 9% significance value, for the MML dataset. At this value, both Amount of Salt and Temperature form partially directed causal links pointing towards Material Loss. Amount of Salt and Temperature are observed to be the dominant factors accelerating the Material Loss because the salt deposits initiate the breaking of the protective layer of the base material and high operating temperature facilitates such corrosion mechanisms. There is a possibility that the inclusion of variables like partial pressure would have addressed the presence of the unmeasured

confounder at LTHC (700°C). This is because LTHC is a function of temperature and partial pressure, as discussed in section 1.1.2.

For the LML condition in Table 6, the undirected causal link with “o” ends formed between Amount of Salt and Material Loss at 1% significance value suggests that at such a low level of material loss, Amount of Salt might have just started to break down the protective layer to cause the Material Loss. Or there is an unmeasured variable that exists which is influencing both variables.

Results beyond the 10% significance level are not discussed since they are not statistically significant.

**TABLE 6** Causal graphs using KCI in FCI algorithm with increasing significance levels for LML dataset

The causal links shown in the previous tables suggest the possible presence of confounding variables. This opens up the avenue to design experiments that also cater to other variables that were not included in this dataset. The FCI algorithm indicates that for the experimental conditions represented in this study's limited dataset, Amount of Salt has the maximum influence on Material Loss.

## 5 | CONCLUSIONS

Understanding the underlying causal mechanisms between the factors leading to hot corrosion in gas turbines can highlight the inner workings of this process. Implementing causal discovery methods can help in recognising the causal relationships between these corrosion factors. These methods were applied to three different datasets that were divided based on the degree of material loss observed on the materials tested: highest, median, and lowest material loss. The causal discovery algorithm FCI was applied to produce the causal graphs that illustrate the causal relationships between the corrosion

variables present in these three datasets. A wide range of significance levels was analysed, to showcase the confidence level with which the causal relationships were formed between the corrosion variables.

After analysing the causal graphs for the given range of significance levels, it was observed that the number of causal links decreased in the order of highest to lowest material loss. As the degree of material loss decreased to the median range, only two causal links i.e., Amount of Salt and Temperature to Material Loss were formed within the set range of significance levels. Eventually, only a single undirected causal link was formed between Amount of Salt and Material Loss for LML conditions. This showcased that there is uncertainty in claiming the real causal relationship between the two variables at low degrees of material loss. Causal graphs produced using the FCI algorithm suggested the possible existence of unmeasured confounding variables.

From this nascent-stage study of causality in hot corrosion, it can be concluded that Amount of Salt and Temperature were the typical factors causing Material Loss from an overall perspective. However, HCl also proved to be a dominant factor for the HML dataset. As this dataset can include pitting regions this can give insight into factors driving pit formation rather than more average metal loss.

The FCI algorithm proved beneficial in understanding the causal relationships, but a randomised and uncontrolled type of corrosion dataset can further help in future causal research.

Since this study is at a nascent phase of its research timeline, several avenues for future research can be delved into to improve the understanding and application of causal discovery techniques. Following are the recommendations that can potentially improve the quality of further studies:

1. A randomised dataset which can help in performing a more comprehensive causal discovery study should be produced.
2. Including variables such as partial pressures of the gaseous contaminants, crystalline structures, and varying gas compositions can improve the depth of the dataset.
3. The sample sizes must be increased to generate stronger causal links with higher confidence levels.
4. If a time-dependent dataset is produced, causal discovery algorithms for time series data can be implemented such as Granger Causality-based algorithms<sup>[30]</sup>.

These recommendations can help in designing the next phase of the causal discovery study of hot corrosion. Expanding upon this study can further help in developing predictive maintenance and material degradation detection models.

## Data Availability Statement

The data that support the findings of this study are available from the corresponding author upon reasonable request.

## References

- [1] Richard T. C. Harman, *Applications for Gas Turbine Engines*, Macmillan Education UK, London, **1981**, pp. 18–33.
- [2] N Eliaz, G Shemesh, RM Latanision, *Engineering failure analysis* **2002**, 9 (1), 31–43.
- [3] Fred Pettit, *Oxidation of Metals* **2011**, 76, 1–21.
- [4] Judea Pearl, *Causality*, Cambridge university press, **2009**.
- [5] Clark Glymour, Kun Zhang, Peter Spirtes, *Frontiers in genetics* **2019**, 10, 524.
- [6] Nageswara Rao Muktinutalapati, *Advances in gas turbine technology* **2011**, 23.
- [7] Joy Sumner, Adriana Encinas-Oropesa, Nigel J Simms, John R Nicholls, *Oxidation of Metals* **2013**, 80, 553–563.
- [8] PW Schilke, *GE Energy* **2004**.
- [9] Stefano Mori, Mathilde Mendil, Jonathan Wells, Neil Chapman, Nigel Simms, Roger Wells, Joy Sumner, *Energy Systems* **2023**, 1–20.
- [10] Roger C Reed, *The superalloys: fundamentals and applications*, Cambridge university press, **2008**.
- [11] Adriana Encinas-Oropesa, Ph.D. thesis, Cranfield University, **2005**.
- [12] Matthew J Donachie, Stephen J Donachie, *Superalloys: a technical guide*, ASM international, **2002**.
- [13] GA Kool, *Journal of Thermal Spray Technology* **1996**, 5 (1), 31–34.
- [14] GW Goward, *Surface and coatings technology* **1998**, 108, 73–79.
- [15] Nadia Vialas, Daniel Monceau, *Oxidation of Metals* **2006**, 66, 155–189.
- [16] WT Wu, A Rahmel, M Schorr, *Oxidation of metals* **1984**, 22, 59–81.
- [17] MJ Pomeroy, *Materials & design* **2005**, 26 (3), 223–231.

- [18] Matej Vuković, Stefan Thalmann, *Journal of Manufacturing and Materials Processing* **2022**, 6 (1), 10.
- [19] Chen Feng, Xiaochen Liu, Shulei Bi, Jian Kang, in *2022 Prognostics and Health Management Conference (PHM-2022 London)*, IEEE, **2022**, pp. 545–548.
- [20] Xia Chen, Jimmy Abualdenien, Manav Mahan Singh, André Borrmann, Philipp Geyer, *Energy and Buildings* **2022**, 277, 112583.
- [21] Xinpeng Shen, Sisi Ma, Prashanthi Vemuri, Gyorgy Simon, *Scientific reports* **2020**, 10 (1), 2975.
- [22] Stephen C. Loftus in *Basic Statistics with R*, Stephen C. Loftus (Ed.), Academic Press, **2022**, pp. 137–150.
- [23] Amitav Banerjee, UB Chitnis, SL Jadhav, JS Bhawalkar, S Chaudhury, *Industrial psychiatry journal* **2009**, 18 (2), 127.
- [24] Jonas Peters, Dominik Janzing, Bernhard Schölkopf, *Elements of causal inference: foundations and learning algorithms*, The MIT Press, **2017**.
- [25] Noel Cressie, Timothy RC Read, *International Statistical Review/Revue Internationale de Statistique* **1989**, 19–43. □
- [26] Alan Agresti, *Categorical data analysis*, Vol. 792, John Wiley & Sons, **2012**.
- [27] Joseph D Ramsey, *arXiv preprint arXiv:1401.5031* **2014**.
- [28] Kun Zhang, Jonas Peters, Dominik Janzing, Bernhard Schölkopf, *arXiv preprint arXiv:1202.3775* **2012**.
- [29] Jenny Yang, Yang Liu, Yufeng Liu, Wei Sun, *The annals of applied statistics* **2021**, 15 (1), 194.
- [30] Uzma Hasan, Emam Hossain, Md Osman Gani, *arXiv preprint arXiv:2303.15027* **2023**.
- [31] Ana Rita Nogueira, Andrea Pugnana, Salvatore Ruggieri, Dino Pedreschi, João Gama, *Wiley interdisciplinary reviews: data mining and knowledge discovery* **2022**, 12 (2), e1449.
- [32] Jiji Zhang, *Artificial Intelligence* **2008**, 172 (16-17), 1873–1896.
- [33] Jiji Zhang, *Journal of Machine Learning Research* **2008**, 9, 1437–1474.
- [34] Judea Pearl, Madelyn Glymour, Nicholas P Jewell, *Causal inference in statistics: A primer*, John Wiley & Sons, **2016**.
- [35] Yangbo He, Jinzhu Jia, Bin Yu, *The Journal of Machine Learning Research* **2015**, 16 (1), 2589–2609.
- [36] Thomas Richardson, Peter Spirtes, *The Annals of Statistics* **2002**, 30 (4), 962–1030.
- [37] Emilija Perkovic, in *Conference on Uncertainty in Artificial Intelligence*, PMLR, **2020**, pp. 530–539.
- [38] Jin Tian, *arXiv preprint arXiv:1207.1428* **2012**.
- [39] Zhongyi Hu, Robin Evans, in *Conference on Uncertainty in Artificial Intelligence*, PMLR, **2020**, pp. 739–748.
- [40] P. Spirtes, C.N. Glymour, R. Scheines, *Causation, Prediction, and Search*, of *Adaptive computation and machine learning*, CogNet, **2000**.
- [41] Yujia Zheng, Biwei Huang, Wei Chen, Joseph Ramsey, Mingming Gong, Ruichu Cai, Shohei Shimizu, Peter Spirtes, Kun Zhang, *arXiv preprint arXiv:2307.16405* **2023**.
- [42] Peter Viklund, Rachel Pettersson, *Oxidation of metals* **2011**, 76 (1-2), 111–126.